Available online at www.sciencedirect.com

SciVerse ScienceDirect

Procedia Engineering 58 (2013) 147 – 156

Procedia Engineering

www.elsevier.com/locate/procedia

The 12th Hypervelocity Impact Symposium

Experimental Studies of Rod Impact on Bare/Uncovered PBX 9501 Explosive

R. L. Gustavsen,* D. M. Dattelbaum, C. E. Johnson, and B. D. Bartram

Los Alamos National Laboratory, Los Alamos NM 87545 USA

Abstract

We present an experimental investigation of the dynamics of rod impact on bare or uncovered PBX 9501 explosive. By weight, PBX 9501 contains 95% octahydro-1,3,5,7-tetranitro-1,3,5,7-tetrazocine, commonly known as HMX. The plastic binder is Estane combined with a nitro-plasticizer made of bis(2,2-dinitropropyl)acetal and bis(2,2-dinitropropyl)formal. Experiments were conducted using our single stage gas-gun, allowing us to get very repeatable impact velocities. A stainless steel rod attached to the front of the projectile impacted the explosive target. Impact occurred while the projectile was still in the barrel, allowing for accurate centering of the rod on the target. Seven channels of Photonic Doppler Velocimetry (PDV) were used to measure shock waveprofiles after transmission through the explosive. Velocimetry measurement points were located at different radii from the center of the rod, allowing us to capture the 2-D characteristics of the flow. Also, multiple sets or sequences of experiments were performed. Each set of experiments used a constant rod diameter, impact velocity and PDV probe locations: the thing that was varied from experiment to experiment was the thickness of the PBX 9501 explosive sample. In this way, we built up a detailed experimental record of the impact and reaction dynamics. All experiments discussed used a rod impact velocity near 0.744 km/s resulting in an impact stress of ~ 4.5 GPa. One series of experiments with 17 mm diameter rods resulted in initiation with onset of detonation between 6 and 8 mm into the explosive. Another series of experiments with 8.5 mm diameter rods resulted in failure to detonate, reactions being quenched by rarefaction waves emanating from the edge of the rod.

Selection and peer-review under responsibility of the Hypervelocity Impact Society

Keywords: Shock initiation, rod impact, plastic bonded explosive, short shock.

1. Introduction

"Bullet" tests[1] have a great deal of relevance for problems of explosive safety. Projectiles with cylindrical symmetry and measured velocity, u_{imp}, are fired from a gun at an explosive test sample. Results are recorded as a "go" meaning detonation, or "no-go" meaning no detonation. Typically, the projectile size and shape is fixed, and the test is repeated with varying bullet velocities in order to determine a velocity threshold at which there is a 50% probability of initiating detonation. This velocity is called the threshold velocity.

Instrumentation for bullet tests has usually been very simple. First, the projectile velocity is measured. Secondly, a measurement of detonation or non-detonation is made. Methods for inferring a go have often been quite simple; a dent in a metal witness plate[2], or the flash generated by a pressure sensitive "paint." More sophisticated techniques measure shock transit times using piezo or electrical shorting pins.[3] Detonation is assumed if detonation velocities are reached. High-speed photography has also been used, both to measure the projectile velocity and to see evidence of reaction and detonation. [4, 5]

* Corresponding author. Tel.: 505-500-2450; fax: 505-667-6372.
E-mail address: rgus@lanl.gov.

1877-7058
Selection and peer-review under responsibility of the Hypervelocity Impact Society
doi:10.1016/j.proeng.2013.05.018

In planar shock initiation experiments, a great deal of energy has been invested in measuring the flow field produced by the reacting explosive. Examples include pressure gauges[6, 7], magnetic particle velocity gauges[8-10], and velocity interferometry[11-14]. These kinds of measurements are often used to calibrate reactive burn models[15-18] used to make direct numerical simulations of initiation and detonation. By contrast, in measurements of projectile impact on explosives, very little effort has gone into measuring details of the flow field. In this study we attempt to rectify this shortfall by making detailed measurements of the flow field.

1.1. Flow resulting from impact of a flat-nosed rod

Following the work of Hugh James[19] we present a "cartoon" of a flat nosed rod about to impact an explosive (Fig. 1a) and the flow resulting from that impact (Fig. 1b). We note that these cartoons are not to scale and represent a simplification of the flow. A rod impacting a target end-on generates a diverging two-dimensional shock wave in the target. If the rod is a right circular cylinder or "flat-nosed," there will be a period of time, shortly after impact, during which the flow in the central part of the shocked volume is 1-D and constant pressure. This is marked "Region of 1-D compression" on Fig 1b.

The shock pressure, or more precisely the longitudinal stress, in the region of 1-D compression can be calculated using the impedance matching method.[20] In this method, the pressure, P and particle velocity, u_p at the interface of the rod and the explosive target must be equal. Using the subscript "1" to denote the explosive target and "2" to denote the rod we have,

$$P_1 = \rho_{0,1} U_{S,1} u_p = P_2 = \rho_{0,2} U_{S,2} \left(u_{imp} - u_p \right) \tag{1}$$

In Equation (1), ρ_0 is the density at zero pressure, u_{imp} is the rod impact velocity, and U_S is the shock velocity. We use linear $U_S - u_p$ equations of state

$$U_S = C_0 + S u_p \tag{2}$$

for both the explosive and the rod. In Eq. (2), C_0 and S are constants specific to the material. The solution to Equations (1) and (2) allows us to compute P, U_S, and u_p in the region of 1-D compression.

After the initial impact, rarefaction waves spread into the 1-D compression region reducing the pressure. In Fig. 1, this is indicated by the arrows pointing horizontally inward with the label "C_b." C_b is the bulk sound speed in the compressed material. At the leading edge of the rarefaction the sound speed can be calculated as

$$C_b = V \left\{ \left(\frac{dP}{dV} \right)_{Hugoniot} \left[\left(V_0 - V \right) \frac{\Gamma}{2V} - 1 \right] + P \frac{\Gamma}{2V} \right\}^{1/2} \tag{3}$$

In Eq. (3), P and V are the pressure and specific volume in the shocked state and V_0 is the specific volume in the un-shocked state. Γ is Gruneisen parameter, $\Gamma = V \left(\partial P / \partial E \right)_V$. In Eq. (3), the subscript "Hugoniot" means that the derivative is calculated on the Hugoniot. Using the Hugoniot jump condition

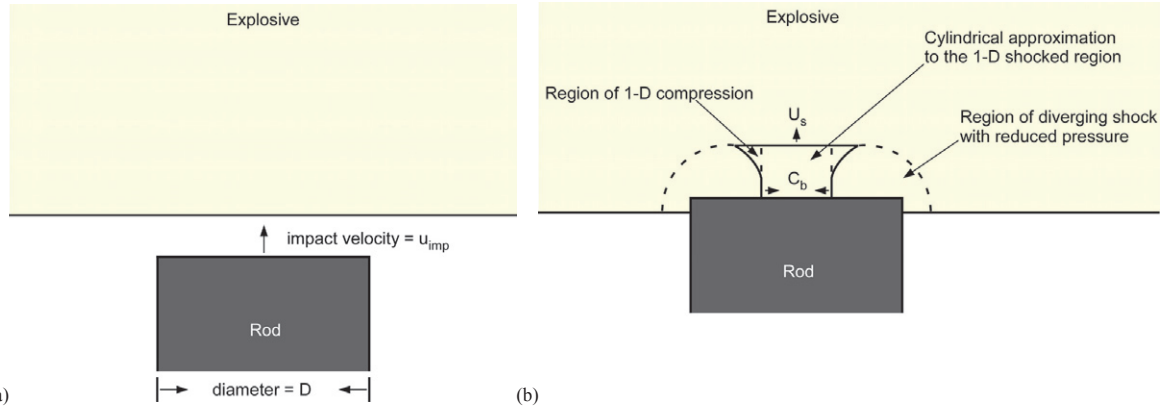

Fig. 1. Schematic representation of (a) the rod tip about to impact the explosive and (b) the flow field in the explosive shortly after impact. (After James[19]).

$$\frac{V}{V_0} = 1 - \frac{u_p}{U_S} \tag{4}$$

with the identity

$$\eta = 1 - \frac{V}{V_0}, \tag{5}$$

the pressure on the Hugoniot can be put in the form

$$P_{Hugoniot} = \frac{\rho_0 \eta C_0^2}{(1 - \eta S)^2}. \tag{6}$$

The derivative of pressure with respect to volume on the Hugoniot is then

$$\left(\frac{dP}{dV}\right)_{Hugoniot} = \rho_0^2 C_0^2 \frac{(1 + \eta S)}{(1 - \eta S)^3}. \tag{7}$$

In computing the sound speed in Eq. (3), we also make the assumption

$$\frac{\Gamma}{V} = \frac{\Gamma_0}{V_0} = const. \tag{8}$$

A final note is that we can only calculate flow parameters analytically in the region of 1-D compression. The bulk sound speed at the leading edge of the rarefaction is just at the boundary of this region. Despite these shortcomings, we have found the framework of Fig. 1 and the equations above to be useful for understanding the problem.

The dynamics illustrated in Fig. 1 and to which Equations (1 – 8) apply are complicated by the release of chemical energy. When shocked above a threshold pressure, an explosive begins to release energy. This energy amplifies the strength of the shock wave. Pressure, particle velocity, and shock velocity all increase as functions of time and the distance the wave propagates into the explosive. If the rarefaction wave, indicated by C_b is spreading into the shocked volume, this has the effect of slowing or quenching the reaction. There is therefore a competition between reactive growth and quenching due to rarefactions.

A final complication is that, at the edge of the rod there is a region of high shear displacement. An idealization is that material in front of the rod face is moving straight ahead and material to the side is stationary. At the boundary is a region of high shear displacement that could get very hot due to frictional or viscous heating. The hot region could serve as an additional site for energy release.

We propose to differentiate between shear initiation and short duration shock initiation as follows. If the time and distance for onset of detonation are similar to those produced by planar shocks of the same impact pressure and duration, we will claim that the dominant mechanism is ordinary shock initiation. For a hypothetical example consider a planar experiment with impact pressure of 4 GPa and duration of 0.5 μs that results in distance and time to detonation of 10 mm and 2 μs. If the flat nosed rod experiment has the same impact pressure of 4 GPa and duration of 0.5 μs and results in distance and time to detonation of 10 mm and 2 μs, we will claim that the results are similar and the influence of shear is minimal. By contrast, if the rod impact results in distances and times to detonation that are a lot less than those produced by planar shocks of the same duration, we will claim that shear accelerates the release of chemical energy and is an important initiation mechanism.

2. Experimental Details

Figure 2 shows the overall experimental configuration. A flat nosed rod is mounted on/in a projectile driven by our 71 mm diameter bore single stage gas gun. The rod impacts a disk of explosive backed by a window. The experiment is repeated holding the rod diameter and velocity constant but with different thicknesses of explosive. The velocity of the explosive/window interface is measured using multi-point velocity interferometry.[21] In this way we assemble detailed 2-D measurements of how the reactive flow evolves as it propagates deeper into the explosive sample.

Use of the gas gun has two advantages. First, all of the experiments in this study used the same impact velocity or as close to that as we could get. In gas guns, projectile velocity is very repeatable from one experiment to the next, typically to within < 1-2 %. Second, because the projectile is in the gun barrel at impact, the target and diagnostics can be aligned quite precisely relative to the rod. We estimate that the target is centered on the barrel within about 0.5-1 mm.

Flat nosed rods were machined from SAE grade 304 stainless steel (nominally 72 % Fe/ 18%Cr/ 10%Ni). We did two series of experiments with rod diameters of 8.5 and 17 mm. Rods were 25.4 mm long, as measured from the flat surface of the projectile to the rod tip.

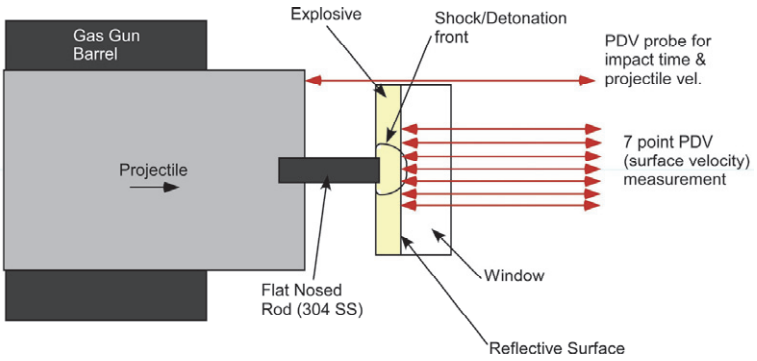

Fig. 2. Configuration for flat nosed rod impact experiments.

The explosive used in these experiments was PBX 9501. This is a composite formed of HMX explosive crystals held together with plastic binder. The mean size of the explosive crystals is about 150 μm and there is a broad distribution of sizes in a typical sample. A micrograph of a typical sample can be seen in Skidmore et al.[22] The PBX 9501 was hot pressed in steel dies from powder lot BAE045145-008. Typical density was 1.833 g/cm^3. Because Theoretical Maximum Density (TMD) for PBX 9501 is 1.860 g/cm^3,[23] samples contained about 1.5% void. Void percentage and the explosive origin, tracked by the lot number, are important factors controlling shock sensitivity.

Explosive samples were in the form of 50.8 mm diameter disks that ranged from 3 – 12 mm thick. Holding everything else constant, at different sample thicknesses the wave will have evolved to different shapes. That is, the wave will either be growing in amplitude and building toward detonation or shrinking in amplitude and tending toward failure. Using different explosive thicknesses this evolution can be recorded.

The reflective surface between the PBX 9501 explosive and the window was 6 μm thick aluminum foil. Foil was obtained from All Foils, Inc. (www.allfoils.com). One side of these foils has a shiny finish and the other side has a matte finish. The side with the matte finish was oriented toward the window. We found it important to use diffuse reflectors in these experiments. The diverging part of the shock wave is curved and use of a specular reflector results in little light being returned to the probe. One experiment with a vapor plated specular reflector lost all light as soon as the shock reached the reflector. The matte finish aluminum reflectors, by contrast, returned sufficient light even after shock arrival.

The window was polymethylmethacrylate (PMMA) 50.8 mm diameter by 12.7 mm thick. PMMA was either Rohm and Haas type II UVA Plexiglas or Polycast (www.spartech.com/polycast.html) PMMA made to Mil-Spec P5425D. The two brands of PMMA are equivalent according to their specifications. Both surfaces of the PMMA window were diamond turned resulting in flat, parallel surfaces with optical quality finishes.

The velocity of the reflector at the PBX 9501/PMMA interface was measured using Photonic Doppler Velocimetry (PDV).[21] PDV is a velocity interferometer that uses 1550 nm light generated by fiber lasers. The interferometer is constructed mainly from single mode fiber optic components that are widely used for long-haul fiber optic based communication applications.

Velocity was measured at 7 different radial locations on the back of the sample. The PDV probes we used are made by AC Photonics, Inc. (www.acphotonics.com, part # 1CL15P020LCC01) This is a collimating probe with a working distance or beam waist at 20 mm. The spot size is typically 150 μm. The probes are housed in brass tubes that are 2.4 mm in diameter. This means that probes can be placed as close as 2.4 mm apart. As shown in Fig. 2, for this series of experiments we placed the probes symmetrically about the rod axis at nominal distances of 0, ± 3, ± 7, and ± 12 mm.

An eighth PDV probe extended in front of the explosive sample about 25.4 mm. This probe was used firstly to measure the projectile velocity. Secondly, the projectile impacted the probe at nominally the same time as the rod impacted the explosive sample. Using this method, we were able to cross-reference all the PDV velocity measurements to the impact time.

Note that we measured the time differences between all 8 PDV channels to within 1 ns. This should not be taken to imply that we know impact time to 1 ns as we will now explain. First, we only know the length of the stainless steel rod and the length of the impact probe to within $\approx 10 \mu m$. With an impact velocity of 0.75 km/s this would correspond to $\approx$7.5 ns. Secondly, typical projectile/target impact tilt for this gun is 1 mrad. Combining this with the 29.2 mm radius of the impact probe results in an impact time uncertainty of $\approx$ 22 ns due to tilt. Combining these, the aggregate uncertainty in impact time is $\approx \pm 30$ ns.

Figure 3 shows photographs of an actual assembly. Figure 3a shows a typical projectile with a flat nosed rod impactor at the muzzle of the gun barrel. The structure on the left of the gun barrel is an optical beam interrupt system used as a redundant method for measuring projectile velocity.

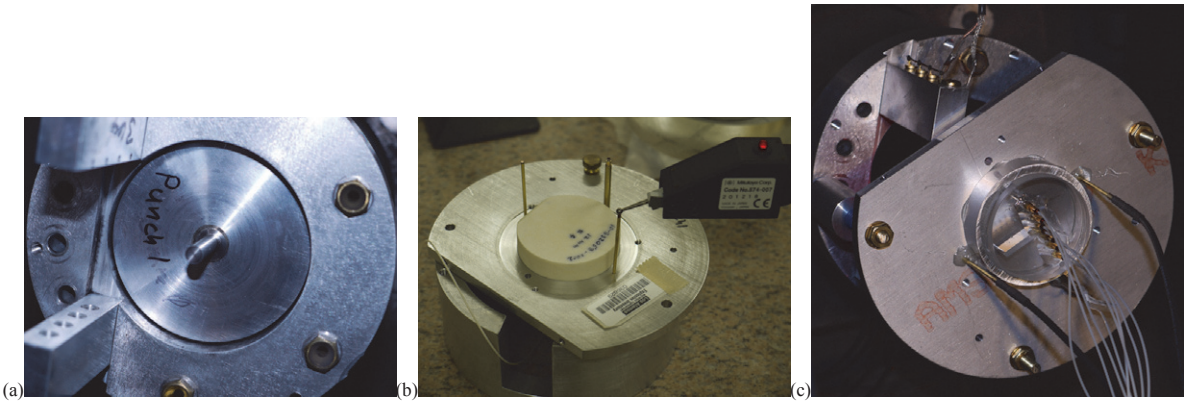

Fig. 3. Photographs of the experiment: (a) projectile with flat nosed rod mounted in the gas-gun barrel, (b) impact face of instrumented target, and (c) back face of target.

Figure 3b shows the impact face of the target. The PBX 9501 explosive is the creamy white disk in the center. To either side are piezoelectric (PZT) pins, which are used to trigger the recording oscilloscopes. The third "pin", located toward the back and center is a PDV probe. It is used both to measure the projectile velocity and, when the projectile impacts it, to generate a signal which can be time correlated with the other PDV probes. The heights of the PZT pins and of the PDV pin are set to impact the projectile when the rod impacts the explosive. A height gauge used to measure the height of the PDV probe and pins is seen on the right of Fig. 3b.

Figure 3c shows the back of a target where it is mounted at the muzzle of our gas gun. Fibers (white) are connected to the 7 PDV probes. The probes are housed in brass tubes that, in turn, are mounted in a PMMA holder attached to the back of the window. The PDV probes transmit and collect 1550 nm laser light onto/from the interface of the explosive and PMMA window. The structure on the top/ left is part of the optical beam interrupt projectile velocity measuring system.

3. Results

Summary data from eight experiments is shown in Table 1. The shot number serves as a unique identifier for the experiment. After that, shots are grouped by the rod diameter and sample thickness. Other data in Table 1 are the PBX 9501 density, the impact velocity, the impact pressure, and a note on whether or not detonation was reached. Shots 1s-1493 and 1s-1490 were building toward detonation, but detonation had not been achieved within the thickness of the explosive. Hence, the notation in the "Detonation" column is "Not yet." Impact pressure and bulk sound speed were calculated using Equations (1 – 8). Equation of state parameters used for the stainless steel rod and PBX 9501 are listed in Table 2.

Table 1. Summary of experiments.

Shot #	Rod diameter (mm)	PBX 9501 Thickness (mm)	PBX 9501 Density (g/cm^3)	Impact vel. (km/s)	Impact Pressure (GPa)	Sound speed (km/s)	Detonation?
1s-1493	16.99	2.986	1.829	0.737	4.41	4.78	Not yet
1s-1490	17.00	5.996	1.835	0.740	4.50	4.81	Not yet
1s-1494	16.98	8.009	1.833	0.738	4.47	4.80	Y
1s-1489	17.02	12.006	1.832	0.740	4.49	4.81	Y
1s-1500	8.55	2.992	1.830	0.743	4.51	4.82	N
1s-1499	8.90	6.005	1.834	0.753	4.60	4.86	N
1s-1501	8.54	8.007	1.835	0.743	4.51	4.82	N
1s-1502	8.80	12.004	1.837	0.744	4.53	4.82	N

Table 2. Equation of State parameters used in Equations (1 – 8).

Material	ρ_0 (g/cm^3)	C_0 (km/s)	S	Γ
PBX 9501[24]	1.835	2.4	2.4	1
304 Stainless Steel[25]	7.926	4.48	1.51	2.18
PMMA < 5 GPa	1.186	2.76	1.42	0.97

Figure 4 shows the results of a single experiment; shot 1s-1500. In this experiment, an 8.55 mm diameter stainless steel rod impacted 2.992 mm of PBX 9501 at 0.743 km/s producing a stress of 4.51 GPa at the rod tip. The results shown in Fig. 4 are in the form of interface velocity vs. time waveprofiles. Seven waveprofiles are obtained in each experiment; the legend indicates the measured distance of the probe from the centerline of the target and rod. At the center (black profile) the profile takes the form of a shock with a very fast rise. This is followed by a rounded "hump." Note that the amplitude of the shock (0.85 km/s) is greater than the rod impact velocity (0.743 km/s). This is one indication of energy release in the explosive, a shock front that grows at it propagates into the sample.[26] The other feature indicating energy release is the rounded hump.

Note that the amplitude of the shock cannot be explained simply by the different impedances. Using the EOS values shown in Table 2, results in an interface particle velocity of 0.738 km/s, less than the 0.85 km/s which was observed.

Off of the centerline, at ± 3 mm (red and pink traces) the shock arrives at the same time as at the center. The magnitude of the shock, however, is reduced. This is partly due to rarefactions from the edge of the rod reducing the pressure behind the shock front. These would arrive very shortly after the initial shock. The other reason the amplitude is reduced is that the PDV probes measure the component of velocity along the direction of rod motion. Even at this thickness and this close to the centerline the wave is curved and motion is directed partly in the radial direction. The difference between the two profiles from the ± 3 mm probes is likely due to the probes being located at slightly different distances from the centerline.

At $\pm$ 7 mm (dark green and light green traces) a very low amplitude flat topped shock arrives at ≈ 1.5 μs. This is followed by slow rise to a peak amplitude of 0.2 km/s. The reason for the low amplitude is two fold. First, the probe location is well beyond the edge of the rod. The shock is therefore very divergent and divergent shocks weaken as they propagate. Secondly, we are again measuring the component of velocity in the axial direction. This component is reduced from the overall magnitude.

At $\pm$ 12 mm, the shock arrives at about 3 μs. The velocity component in the axial direction is again very weak, about 0.1 km/s.

Figure 5 shows waveprofiles obtained in the two sets of experiments with 8.5 and 17 mm diameter rods. All experiments are shown on a single plot so that comparisons are easy to make. From Table 1, we note that the impact velocity, and therefore the impact pressure, was nearly the same in all experiments. What varied was the rod diameter and the explosive thickness.

In Figure 5, going top to bottom within a column, the rod diameter is held constant and the explosive thickness increases. Using this, you can visualize the flow as the shock travels through more and more explosive. Thus, Figs. 5a – 5d track the flow generated by impact of a 17 mm diameter rod onto 3, 6, 8, and 12 mm of explosive. In similar manner, figs. 5e—5h displays the flow generated by impact of an 8.5 mm diameter rod onto 3, 6, 8, and 12 mm of explosive. Going left to right within a row, the explosive thickness is held constant while the rod diameter changes. Thus, the effect of rod diameter can be examined at any thickness.

In Figs. 5a – 5d, we see a wave that is evolving toward detonation. Detonation begins between the depths of 6 mm and 8 mm. At the 8 mm depth (Fig. 5c) waveprofiles from the center of the sample (0, ± 3 mm) take the form of right triangles with a peak amplitude of > 3 km/s. The right triangle waveforms with peak velocity > 3 km/s are a signature of detonation. Also in Fig. 5c, we see that at radii of ± 7 mm and ± 12 mm detonation has not yet been achieved. The shock followed by a hump type of profile is still evident. This indicates that at the larger radii, the shock is still building toward a detonation.

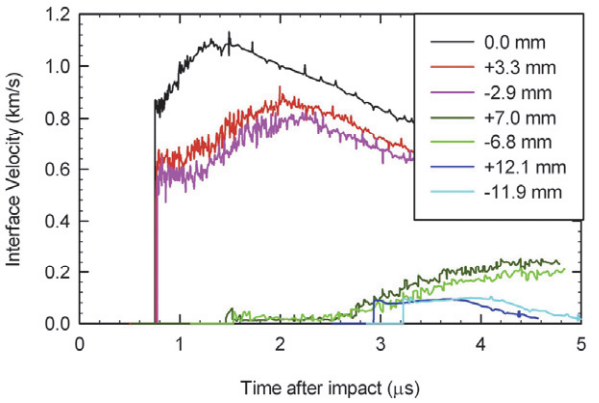

Fig. 4. Result for shot 1s-1500; 8.55 mm stainless steel rod impacting 2.992 mm of PBX 9501 at 0.743 km/s. The legend shows the positions of the PDV probe beams relative to the centerline.

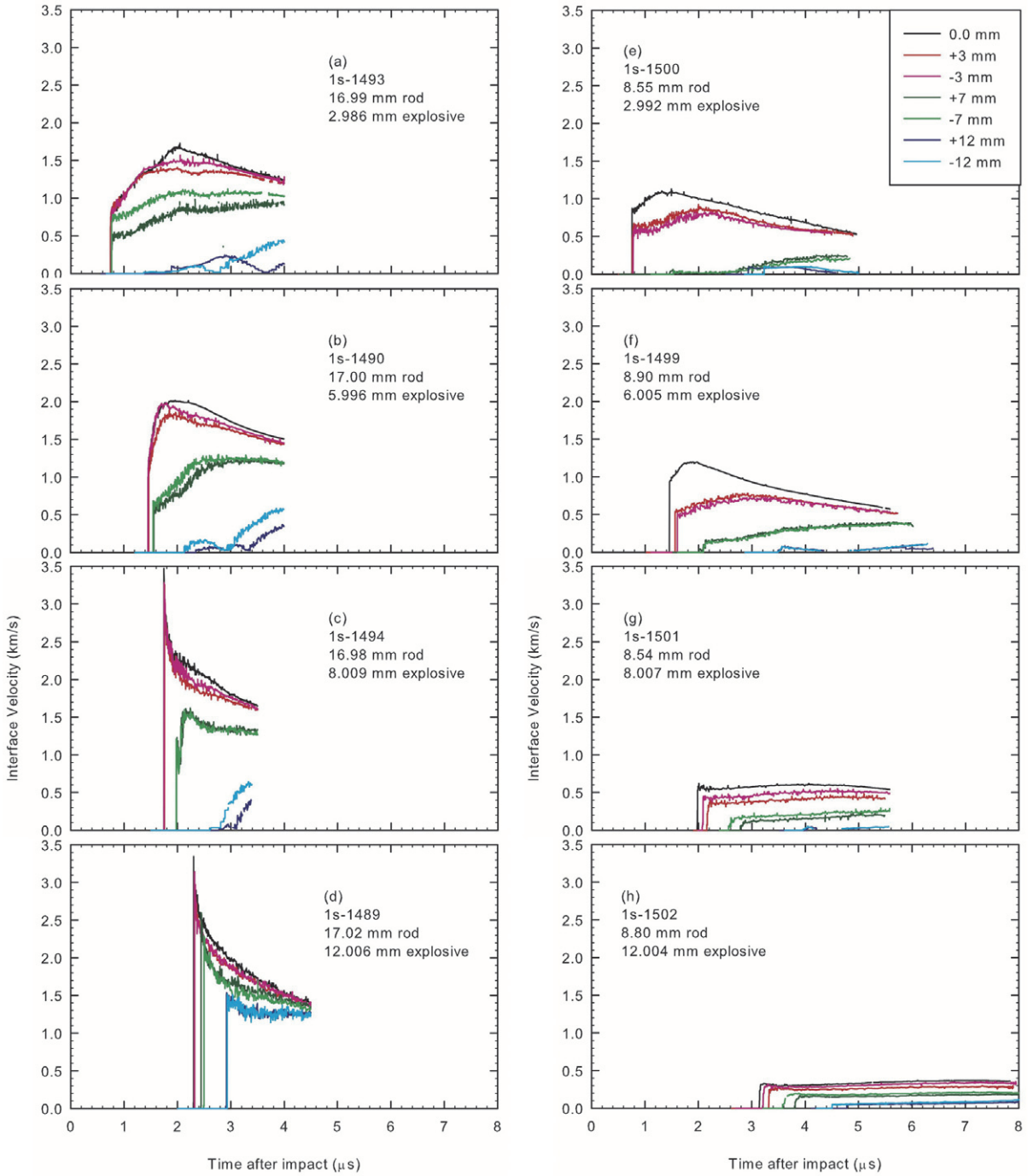

Fig. 5. Wave profiles generated using 17.0 mm diameter rods (a – d) and 8.5 mm diameter rods (e – h). The legend in plot (e) applies to all plots and indicates the nominal distance the PDV probe is from the centerline. Note also that the velocity recorded is the component in the direction of projectile motion.

Prior to the onset of detonation, In Figs. 5a – 5b we see wave profiles that are typical of shock initiation in heterogeneous explosives. By heterogeneous explosives we mean explosives with a microstructure. These include typical pressed and plastic bonded explosives. The microstructure comes from the explosive being made of grains which are pressed and bonded together. Heterogeneous explosives can be contrasted with homogeneous explosives such as liquids. In liquids there is no microstructure. Initiation behavior in liquid explosives, and the resulting waveprofiles are distinctly different

than those seen in heterogeneous explosives.[27-29] Microstructure can be introduced into liquid explosives by adding in particles such as glass beads or glass micro-balloons.[30, 31]

Features of the wave profiles in initiating heterogeneous explosives are the following:

- The shock front increases in amplitude as the wave travels deeper into the explosive.
- Following the shock front is a rounded "hump" which is larger in amplitude than the shock front.
- Like the shock front, the hump grows in amplitude as the wave progresses through the explosive.
- The hump eventually overtakes the shock front. Detonation onset is approximately simultaneous with this event.
- After the hump overtakes the front, the triangular waveprofiles appear indicating detonation.

In summary, the sequence of waveprofiles seen in Figs. 5a – 5d is clearly typical of initiation in a heterogeneous explosive. Furthermore, the profiles are very similar to those recorded using embedded gauges in PBX 9501.[24, 32]

From Table 1, the average density of the PBX 9501 samples is 1.833 g/cm^3. Gibbs and Popolato tabulated explosively driven wedge test data for PBX 9501 at this density.[23] This data was in the form of initial shock pressure, P, vs. x_d and t_d the distance and time to onset of detonation respectively. We have fit this data to a power law with result;

$$x_d = 51.2P^{-1.41} \text{ mm}, \tag{9}$$

$$t_d = 17.9P^{-1.67}\ \mu s. \tag{10}$$

(Note that the power law when put in Log – Log form is a straight line. This is the way Pop-plots are usually presented. Using the average initial shock pressure of $P = 4.50$ +/- 0.05 GPa, we find coordinates for onset of detonation to be x_d = 6.1 $\pm$ 1.0 mm, t_d = and 1.44 $\pm$ 0.25 μs. (The error bars shown are based on the 95% confidence interval.) In Figs. 5a – 5d we saw detonation begin between 6 and 8 mm. This is consistent with the planar shock Pop-plot for PBX 9501 at this density.

By contrast with the waveprofiles produced by 17 mm diameter rods (Figs. 5a-5d), waveprofiles produced by 8.5 mm diameter rods (Figs. 5e-5h) show initiation beginning and then failing. The initial shock front in the center and after transmission through 3 mm of HE is about the same; 0.9 km/s (compare Figs. 5a and 5e). After that, for the 8.5 mm rod, the hump is lower than it is for the 17 mm rod. This is due to rarefactions from the edges of the rod coming into the flow. In fact, using the cylindrical approximation shown in Fig. 1 to calculate where the rarefaction is, we see that for the 17 mm rod rarefactions cross the 7 mm radius at 0.3 μs, the 3 mm radius at 1.1 μs, and reach the center at 1.8 μs. By contrast, for the 8.5 mm rods, the rarefaction crosses the 3 mm radius at 0.3 μs, and reaches the center at 0.9 μs. It is this intrusion of the rarefaction wave into the planar shock region that causes the initiation to fail.

4. Discussion

According to Hugh James and his collaborators,[19, 33-35] initiation by flat nosed rods is a short duration shock phenomena. Planar short duration shock experiments typically use the impact of thin flyer plates onto an explosive.[36, 37] A shock is driven forward into the explosive and backward into the flyer. When the shock reaches the back of the flyer, a rarefaction is generated. The rarefaction then travels forward through the flyer and into the explosive. Eventually, the rarefaction *may* overtake the shock front. If overtake occurs prior to the beginning of detonation, the beginning of detonation may be delayed or detonation may not be achieved.

Walker and Wasley,[37] have found that there is a critical energy E_c, for initiation. This is given by

$$E_c = Pu_p\tau, \tag{11}$$

where τ is the time duration of the shock. For energies greater than the critical energy, detonation is achieved. For energies less than the critical energy, detonation is not achieved. Critical energy can be achieved with a high-pressure short duration shock or with a low-pressure shock of long duration.

Unfortunately, the critical energy for PBX 9501 has not been measured. A similar explosive, PBX 9404, contains 94 wt. % HMX, and a plastic binder of 3 wt. % nitrocellulose, and 3 wt. % chloroethylphosphate.[23] The critical energy for PBX 9404 is 0.64 MJ/m^2.[38] Using this value in Eq. (11), together with the average pressure of 4.50 GPa and the average particle velocity of 0.628 km/s we find a critical time estimate of $\tau_c = 0.23\mu s$ for shocks of 4.5 GPa.

James[19] has adapted the critical energy criterion summarized by Eq. (11) to rod impact. For rod impact, the shock duration τ is replaced by the time at which the volume of 1-D shock compression is a maximum. From Fig. 1b it is straightforward to compute the volume of 1-D shock compression in the approximation of cylindrical symmetry. This is

$$V_{1\text{–}D} = \left[\left(U_S - u_p\right)t\right]\left[\frac{\pi}{4}\left(D - 2C_b t\right)^2\right] \tag{12}$$

In Eq. (12), D is the rod diameter and t is the time after impact. The derivative of the volume with respect to time can be put in the form

$$\frac{dV_{1\text{–}D}}{dt} = \frac{\pi}{4}\left(U_S - u_p\right)\left(D - 6C_b t\right)\left(D - 2C_b t\right). \tag{13}$$

The maximum volume occurs when $D = 6C_b t$. So for a rod, the effective shock duration is

$$\tau = \frac{D}{6C_b}. \tag{14}$$

Using Eq. (14) we find that $\tau = 0.295\,\mu s$ for the 8.5 mm rods and $\tau = 0.590\,\mu s$ for 17 mm diameter rods. Both of these times are greater than the critical time of 0.23 μs calculated using the critical energy of PBX 9404; $E_c = 0.64$ MJ/m^2.[38] Furthermore, impact of the 8.5 mm rods with $\tau = 0.295\,\mu s$ did not result in detonation. Therefore, for PBX 9501 $E_c > 0.83$ MJ/m^2. This is a greater critical energy than for PBX 9404[38] and might be expected since PBX 9501 is less shock sensitive than PBX 9404.

On the role of initiation caused by the shear near the edges of the rod, we note that the distance and time to onset of detonation for the 17 mm rod impact (6 mm < x_d < 8 mm and 1.3 μs < t_d < 1.8 μs) are similar to or greater than those obtained for planar 4.5 GPa shocks of long duration; namely 6.1 mm and 1.44 μs. From this we conclude that shear is not a dominant factor in initiation for 17 mm diameter rods with 4.5 GPa impact pressure. The 8.5 mm diameter rods with impact pressure of 4.5 GPa failed to produce detonation within more than 3 μs. This result was in line with the short duration shock initiation response of PBX 9501. Thus we conclude that, shear ignition does not seem to overpower the shock initiation response in this impact pressure and time regime.

Our finding that shock initiation is the dominant response was obtained with the following limitations. First of all, we were looking for a response in the shock initiation pressure and time regime; 4.5 GPa and < 5 μs. It may be that shear ignition takes much longer to transit to detonation. In line with this, our explosive samples were of limited size; ≤ 12 mm thick and 50 mm diameter. With the 8.5 mm diameter rods, perhaps, ignition rather than failure would have been observed if the samples had been much larger and observations had been made for longer times.

Lastly we think that these experiments are likely to be most useful as a test for reactive burn models. For example, we did some initial trials using the CTH hydrocode[39] with the History Variable Reactive Burn model.[40] Model parameters were carefully calibrated to reproduce particle velocity waveprofiles in PBX 9501 initiated by sustained and short duration planar shocks.[24] With these calibrations, very good agreement between model and experiment was obtained for sustained shocks and fair agreement was obtained for the short shocks. When applied to the flat nosed rod experiments, the CTH/HVRB simulations produced results that were qualitatively in agreement with experiments in terms of Go-No-Go behavior. That is, detonation was predicted for the 17 mm diameter rod and non-detonation was predicted for the 8.5 mm diameter rod. However, calculated waveprofiles did not compare well with measured waveprofiles in even a qualitative sense. Shocks were calculated at times and places where shocks were not observed. Of course there are reactive burn models other than CTH/HVRB. Perhaps another model will produce waveprofiles that are closer to the experimental results. And perhaps this data will serve as a rather severe test for these types of reactive burn hydrocode model.

Acknowledgements

We thank Adam Pacheco and Ben Hollowell for operating the gas gun. We thank Dave Holtkamp for loaning us four channels of PDV. This work was performed under the auspices of the US government, Department of Energy, National Nuclear Security Administration.

References

[1] Dewey, J. M., 1955. Initiation of Military Explosives by Projectile Impact, in "*Second ONR Symposium on Detonation*", Office of Naval Research: Silver Spring, MD, p. 612.

[2] Bahl, K. L., Vantine, H. C., and Weingart, R. C., 1981. The Shock Initiation of Bare and Covered Explosives by Projectile Impact, in "*Seventh Symposium (International) on Detonation*" J. M. Short, Editor, Naval Surface Weapons Center: White Oak, MD, p. 325.

[3] Lappo, K. N., Todd, S. N., Anderson, M. U., and Vogler, T. J., 2007. Non-Shock Initiiation of the Plastic Bonded Explosive PBXN-5: Experimental Results, in "*AIP Conference Proceedings*" M. Elert, M. D. Furnish, R. Chau, N. Holmes, and J. Nguyen, Editors, AIP, p. 959.

[4] Cook, M. D., Haskins, P. J., and James, H. R., 1994. An Investigation of the Response of Secondary Explosives to Conical-Tipped Projectiles and Oblique Impacts, in "*High-Pressure Science and Technology-1993*" S. C. Schmidt, J. W. Shaner, G. A. Samara, and M. Ross, Editors, AIP Conference Proceedings: Woodbury, NY, p. 1421.

[5] Cook, M. D., Haskins, P. J., Briggs, R. I., Flower, H., Ottley, P., Wood, A. D., and Cheese, P. J., 2006. An Investigaton into the Mechanisms Responsible for Delayed Detonations in Projectile Impact Experiments, in "*Thirteenth International Detonation Symposium*" S. Peiris and R. Doherty, Editors, Office of Naval Research: Arlington, VA, p. 814.

[6] Wackerle, J., Rabie, R. L., Ginsberg, M. J., and Anderson, A. B., *A Shock Initiation Study of PBX-9404*, in *Symposium on High Dynamic Pressures,*

Behavior of Dense Media Under High Dynamic Pressures. 1978, Commissariat a l'Energie Atomique, Centre d'Etudes Nucleares de Saclay: Paris, France.
[7] Vantine, H., Chan, J., Erickson, L., Janzen, J., Weingart, R., and Lee, R., 1980. Precision stress measurements in severe shock-wave environments with low-impedance manganin gauges, Review of Scientific Instruments, 51, p. 116.
[8] Erickson, L. M., Johnson, C. B., Parker, N. L., Vantine, H. C., Weingart, R. C., and Lee, R. S., *The Electromagnetic Gauge: Use of Multiple Gauges, Time Response, and Flow Perturbations*, in *Seventh Symposium (International) on Detonation*, J. M. Short, Editor. 1981, Naval Surface Weapons Center: White Oak, MD. p. 1062.
[9] Vorthman, J. E., *Facilities for the Study of Shock Induced Decomposition of High Explosives*, in *Shock Waves in Condensed Matter - 1981*, W. J. Nellis, L. Seaman, and R. A. Graham, Editors. 1981, AIP Conference Proceedings. p. 680.
[10] Sheffield, S. A., Gustavsen, R. L., and Alcon, R. R., 1999. In-Situ Magnetic Gauging Technique used at LANL-Method and Shock Information Obtained, in "*Shock Compression of Condensed Matter - 1999*" M. D. Furnish, L. C. Chhabildas, and R. S. Hixson, Editors, AIP Conference Proceedings: Melville, NY, p. 1043.
[11] Setchell, R. E., 1983. Effects of precursor waves in shock initiation of granular explosives, Combustion and Flame, 54, p. 171
[12] Setchell, R. E., 1981. Ramp Wave Initiation of Granular Explosives, Combustion and Flame, 43, p. 255
[13] Setchell, R. E., *Short pulse shock initiation of granular explosives*, in *Seventh Symposium (International) on Detonation*, J. M. Short, Editor. 1981, Naval Surface Weapons Center: White Oak, MD. p. 857.
[14] Wackerle, J., Stacy, H. L., and Seitz, W. L., *Velocimetry Studies on the Prompt Initiation of PBX 9502*, in *Tenth International Detonation Symposium*, J. M. Short and D. G. Tasker, Editors. 1993, Office of Naval Research: Arlington, VA. p. 468.
[15] Lee, E. L. and Tarver, C. M., 1980. Phenomenological model of shock initiation in heterogeneous explosives, Physics of Fluids, 23, p. 2362.
[16] Wescott, B. L., Stewart, D. S., and Davis, W. C., 2005. Equation of state and reaction rate for condensed phase explosives, Journal of Applied Physics, 98, p. 053514.
[17] Handley, C. A., *The CREST reactive burn model*, in *Thirteenth International Detonation Symposium*, S. Peiris and R. Doherty, Editors. 2006, Office of Naval Research: Arlington, VA. p. 864.
[18] Shaw, M. S. and Menikoff, R., *A Reactive Burn Model for Shock Initiation in a PBX: Scaling and Separability Based on the Hot Spot Concept*, in *Fourteenth International Detonation Symposium*, C. B. S. Peiris and B. Asay, Editors. 2010, Office of Naval Research: Arlington, VA. p. 1487.
[19] James, H. R., 1988. Critical Energy Criterion for the Shock Initiation of Explosives by Projectile Impact, Propellants, Explosives, Pyrotechnics, 13, p. 35.
[20] McQueen, R. G., Marsh, S. P., Taylor, J. W., Fritz, J. N., and Carter, W. J., 1970. The Equation of State of Solids from Shock Wave Studies, in "*High-Velocity Impact Phenomena*" R. Kinslow, Editor, Academic Press: New York, p. 293.
[21] Strand, O. T., Goosman, D. R., Martinez, C., Whitworth, T. L., and Kuhlow, W. W., 2006. Compact System for High-Speed Velocimetry using Heterodyne Techniques, Review of Scientific Instruments, 77, p.
[22] Skidmore, C. B., Phillips, D. S., Howe, P. M., Mang, J. T., and Romero, J. A., 1998. The Evolution of Microstructural Changes in Pressed HMX Explosives, in "*Eleventh International Detonation Symposium*" J. M. Short and J. E. Kennedy, Editors, Office of Naval Research: Arlington, VA, p. 556.
[23] Gibbs, T. R. and Popolato, A., *LASL Explosive Property Data*. 1980, Berkeley, CA: University of California Press.
[24] Gustavsen, R. L., Sheffield, S. A., Alcon, R. R., and Hill, L. G., 2002. Shock initiation of new and aged PBX 9501, in "*Twelfth International Detonation Symposium*" J. M. Short and J. L. Maienschein, Editors, Office of Naval Research: Arlington, VA, p. 530.
[25] Marsh, S. P., *LASL Shock Hugoniot Data*. 1980, Berkeley, CA: University of California Press.
[26] Sheffield, S. A., Gustavsen, R. L., Hill, L. G., and Alcon, R. R., *Electromagnetic gauge measurements of shock initiating PBX 9501 and PBX 9502 explosives*, in *Eleventh International Detonation Symposium*, J. M. Short and J. E. Kennedy, Editors. 1998, Office of Naval Research: Arlington, VA. p. 451.
[27] Campbell, A. W., Davis, W. C., and Travis, J. R., 1961. Shock initiation of detonation in liquid explosives, The Physics of Fluids, 4, p. 498.
[28] Sheffield, S. A., Engelke, R., and Alcon, R. R., 1989. In-situ study of the chemically driven flow fields in initiating homogeneous and heterogeneous nitromethane explosives, in "*Ninth Symposium (International) on Detonation*" E. L. Lee and J. M. Short, Editors, Office of the Chief of Naval Research: Arlington, VA, p. 39.
[29] Sheffield, S. A., Dattelbaum, D. M., Engelke, R., Alcon, R. R., Crouzet, B. L., Robbins, D. L., Stahl, D. B., and Gustavsen, R. L., 2006. Homogeneous shock initiation process in neat and chemically sensitized nitromethane, in "*Thirteenth International Detonation Symposium*" S. Peiris and R. Doherty, Editors, Office of Naval Research: Arlington, VA, p. 401.
[30] Dattelbaum, D. M., Sheffield, S. A., Stahl, D. B., and Dattelbaum, A. M., 2009. Influence of Hot Spot Features on the Shock Initiation of Heterogeneous Nitromethane, in "*Shock Compression of Condensed Matter - 2009*" M. L. Elert, W. T. Buttler, M. D. Furnish, W. W. Anderson, and W. G. Proud, Editors, AIP Conference Proceedings: Melville, NY, p. 263.
[31] Dattelbaum, D. M., Sheffield, S. A., Stahl, D. B., Dattelbaum, A. M., Trott, W., and Engelke, R., 2010. Influence of Hot Spot Features on the Initiation Characteristics of Heterogeneous Nitromethane, in "*Fourteenth International Detonation Symposium*" B. W. Asay, S. Peiris, and C. Boswell, Editors, Office of Naval Research: Arlington, VA, p. 611.
[32] Gustavsen, R. L., Sheffield, S. A., Alcon, R. R., and Hill, L. G., 1999. Shock initiation of new and aged PBX 9501 measured with embedded electromagnetic particle velocity gauges, LA-13634-MS, p.
[33] James, H. R., Cook, M. D., and Haskins, P. J., *The response of homogeneous explosives to projectile attack*, in *Eleventh International Detonation Symposium*, J. M. Short and J. E. Kennedy, Editors. 1998, Office of Naval Research: Arlington, VA. p. 581.
[34] James, H. R., Haskins, P. J., and Cook, M. D., 1996. Prompt Shock Initiation of Cased Explosives by Projectile Impact, Propellants, Explosives, Pyrotechnics, 21, p. 251.
[35] James, H. R., 1996. An Extension to the Critical Energy Criterion Used to Predict Shock Initiation Thresholds, Propellants, Explosives, Pyrotechnics, 21, p. 8.
[36] Gittings, E. F., 1965. Initiation of a solid explosive by a short-duration shock, in "*Fourth Symposium (International) on Detonation*" S. J. Jacobs, Editor, Office of Naval Research - Department of the Navy: Washington, D.C., p. 373.
[37] Walker, F. E. and Wasley, R. J., 1969. Critical Energy for Shock Initiation of Heterogeneous Explosives, Explosivstoffe, 17, p. 9.
[38] Green, L. G., Nidick, E. J., and Walker, F. E., 1974, Critical Shock Initiation Energy of PBX 9404; a New Approach, Report UCRL-51522, Lawrence Livermore National Laboratory.
[39] Hertel, E. S. J., Bell, R. L., Elrick, M. G., Farnsworth, A. V., Kerley, G. I., McGlaun, J. M., Petney, S. V., Silling, S. A., Taylor, P. A., and Yarrington, L., 1993. CTH: A Software Family for Multi-Dimensional Shock Physics Analysis, in "*19th International Symposium on Shock Waves*", p. 377.
[40] Kerley, G. I., 1992, CTH Equation of State Package: Porosity and Reactive Burn Models, Report Sandia National Laboratories.